Journal of the European Ceramic Society 23 (2003) 647–657
www.elsevier.com/locate/jeurceramsoc

Uniaxial plastic deformation in the zirconia-based nanocrystalline ceramics containing a silicate glass

R. Chaim[a,*], R. Ramamoorthy[a], A. Goldstein[b], I. Eldror[c], A. Gurman[c]

[a]*Department of Materials Engineering, Technion-Israel Institute of Technology, Haifa 32000, Israel*
[b]*Israel Ceramic and Silicate Institute, Technion City, Haifa 32000, Israel*
[c]*Metallurgy Group, Engineering Center, Israel Aircraft Industries, Ben-Gurion International Airport 70100, Israel*

Received 1 November 2001; received in revised form 31 May 2002; accepted 16 June 2002

Abstract

Nanocrystalline yttria-stabilized tetragonal zirconia polycrystal (nc-Y-TZP) powders coated with silicate based glasses were cold isostatically pressed and sintered near to the full density (98–99%). Two glasses with different compositions were used: 93 SiO_2–1 Na_2O–6 SrO (mol%) (designated as SNS glass) and 58 SiO_2–29 Al_2O_3–13 SrO (designated as SAS glass). Uniaxial compression tests of the pure (glass-free) nc-Y-TZP samples yielded strain rates as high as $2{\cdot}10^{-4}$ s^{-1} under 60 MPa at 1300 °C. Comparable strain rates were measured in the SNS glass-containing samples, with the maximum of $3{\cdot}10^{-4}$ s^{-1} at 1300 °C under a stress of 80 MPa (5 vol.% SNS glass content). Compression tests under 100 MPa exhibited relatively high strain rates of $5{\cdot}10^{-4}$ and 10^{-4} at 1300 °C and 1200 °C, respectively, in the 15 vol.% SAS glass samples. The strain rates measured in the SAS glass-containing samples were achieved at temperatures lower by 100 °C compared to the similar strain rates in the glass-free and SNS glass-containing samples. The microstructure of the deformed samples was similar to that of samples before deformation, within which the ultrafine and equiaxed character of the grains was preserved. Clear evidence for cooperative grain boundary sliding was observed in the SAS glass-containing samples.

Keywords: Coatings; Composites; Glass; Mechanical properties; Plasticity; TEP; ZrO_2

1. Introduction

Superplastic deformation of ceramics is a well known phenomena which has been mainly related to their ultra-fine grain size.[1–3] However, as was discussed by Dominguez et al.,[4,5] the expected increase by several orders of magnitude in the strain rate due to the grain size refinement was not observed in ultra-fine glass-free ceramics. On the other hand, based on the microstructural observations, there is a general agreement that grain boundary sliding acts as the main mechanism for the superplastic deformation in these ceramics.[6–8] Therefore, engineering of the grain boundary properties such as incorporation of a grain boundary glassy phase with controlled properties should be appropriate for promoting the superplastic deformation characteristics.[9–11]

The present work describes the superplastic deformation behavior of nanocrystalline Y-TZP ceramics that contain varying amounts of two different glass compositions as grain boundary glassy phases.

2. Experimental procedure

2.1. Fabrication of the samples

Commercial nanocrystalline Y-TZP powders (Tioxide) were coated with two different silicate-based glasses through the sol-gel technique. Detailed description of the coating process followed by sintering and the resultant microstructural evolution has been provided elsewhere.[12,13] The glass compositions were determined by X-ray fluorescence spectroscopy to be 93 SiO_2–1 Na_2O–6 SrO (mol%) (designated as SNS glass) and 58 SiO_2–29 Al_2O_3–13 SrO (designated as SAS glass). Appropriate amounts of the coating solution were applied in order to

* Corresponding author. Tel.: +972-4-8294589; fax: +972-4-8321978.
E-mail address: rchaim@tx.technion.ac.il (R. Chaim).

0955-2219/02/$ - see front matter © 2002 Published by Elsevier Science Ltd.
PII: S0955-2219(02)00198-X

reach glass contents of 5, 10 and 15 vol.% in the final compacts.

The nc-Y-TZP powders with and without the glass were compacted into cylindrical pellets of 15×15 mm, followed by cold isostatic pressing at 250 MPa. The 55% dense green compacts were sintered at 1400 °C for 1 h to near full density as summarized in Table 1.

Rectangular specimens of 3 × 3 × 4 mm^3 were cut and used for uniaxial compression tests in the constant load regime. The compression test set-up was heated during 3 h to the deformation temperature. Then, the load was increased in steps at constant temperature. The specimen contraction was recorded within the accuracy of ±2 μm. Compression tests were performed using a homemade machine and within the temperature range 1150–1300 °C. The compressive load was applied to the samples through the alumina rods and SiC pads. The average test duration was about 2.6 h.

According to the high temperature deformation tests, selected specimens were chosen for microstructural characterization prior to and after the deformation using scanning electron microscopy (SEM-XL30) and transmission electron microscopy (TEM-2000FX); the specimens were prepared by conventional techniques.

2.2. Mechanical tests

Application of constant load in uniaxial compression results in a decrease of stress during the plastic deformation. Thus, the superplastic forming (SPF) strain, stress and strain rate are given by:

$$\varepsilon = \ln\left(\frac{h}{h_0}\right) \tag{1}$$

$$\sigma = \sigma_0 \cdot \left(\frac{h}{h_0}\right) \tag{2}$$

and

$$\frac{\dot{\varepsilon}}{\dot{\varepsilon}_0} = \left(\frac{\sigma}{\sigma_0}\right)^{\frac{1}{m}} \tag{3}$$

Table 1
Characteristics of the NC-Y-TZP specimens sintered at 1400 °C for 1 h

Glass content[a] (vol.%)	Relative density (%)	Phase content (%)[b]		Mean grain size (nm)
		t	m	
0	98	100	–	196
5	99	83	17	140
10	98	69	31	110
15	99	74	26	100

[a] SNS glass.
[b] *t* and *m* refer to tetragonal and monoclinic polymorphs, respectively.

where: ϵ— true strain $\dot{\varepsilon}$, h and σ—the time dependent strain rate, height and stress, respectively. $\dot{\varepsilon}_0$, h_0 and σ_0—the initial strain rate, height and stress, respectively. m—the SPF parameter equals the reciprocal of the stress exponent—n.

The solution of this set of equations gives:

$$\frac{h}{h_0} = \left(1 + \frac{\dot{\varepsilon}_0}{mt}\right)^{-m} \tag{4}$$

where: t—time.

At the beginning of each load increase step, the stress is calculated by dividing the load by the actual area, i.e.:

$$\sigma = \frac{P}{S_0} \cdot \frac{h}{h_0} \tag{5}$$

where: P—load, and S_0—the initial area under the stress.

Simultaneously, the strain rate is calculated from the slope of the plot:

$$\dot{\varepsilon} = \frac{\mathrm{d}}{\mathrm{d}t}\left[\ln\left(\frac{h}{h_0}\right)\right] \tag{6}$$

3. Results

3.1. Deformation tests

The strain rate versus stress at different temperatures in pure (glass-free) nc-Y-TZP samples is shown in Fig. 1a. The strain rate increases with temperature and ranges from $5{\cdot}10^{-6}$ to above 10^{-4}. The data points were fitted in the logarithmic scale by lines, the slopes of which (n values, where $n = \frac{1}{m}$) were determined to be about 1.7. However, at 1300 °C and stresses below ~50 MPa the slope was about 4.0. The significance of these slopes is for determination of the deformation mechanisms.

The strain rate–stress diagram for the 15 vol.% SNS glass-containing samples (Fig. 1b) revealed almost similar strain rate values (although slightly higher) with respect to temperature and stress, compared to the pure nc-Y-TZP (Fig. 1a). The slope values were 1.6 and 4.0 at high and low stress levels, respectively.

On the other hand, higher strain rates were recorded at the respective temperatures and stress levels for the 15 vol.% SAS glass-containing samples, as shown in Fig. 1c. Comparison of the last two diagrams (Fig. 1b and c) demonstrates the effect of the glass composition on the strain rate. In the last system, high strain rates (~10^{-4}) were measured at relatively lower temperatures (1200 °C). In addition, the slopes of the linear fits were 0.6 and 1.7 at the lower and higher temperatures, respectively.

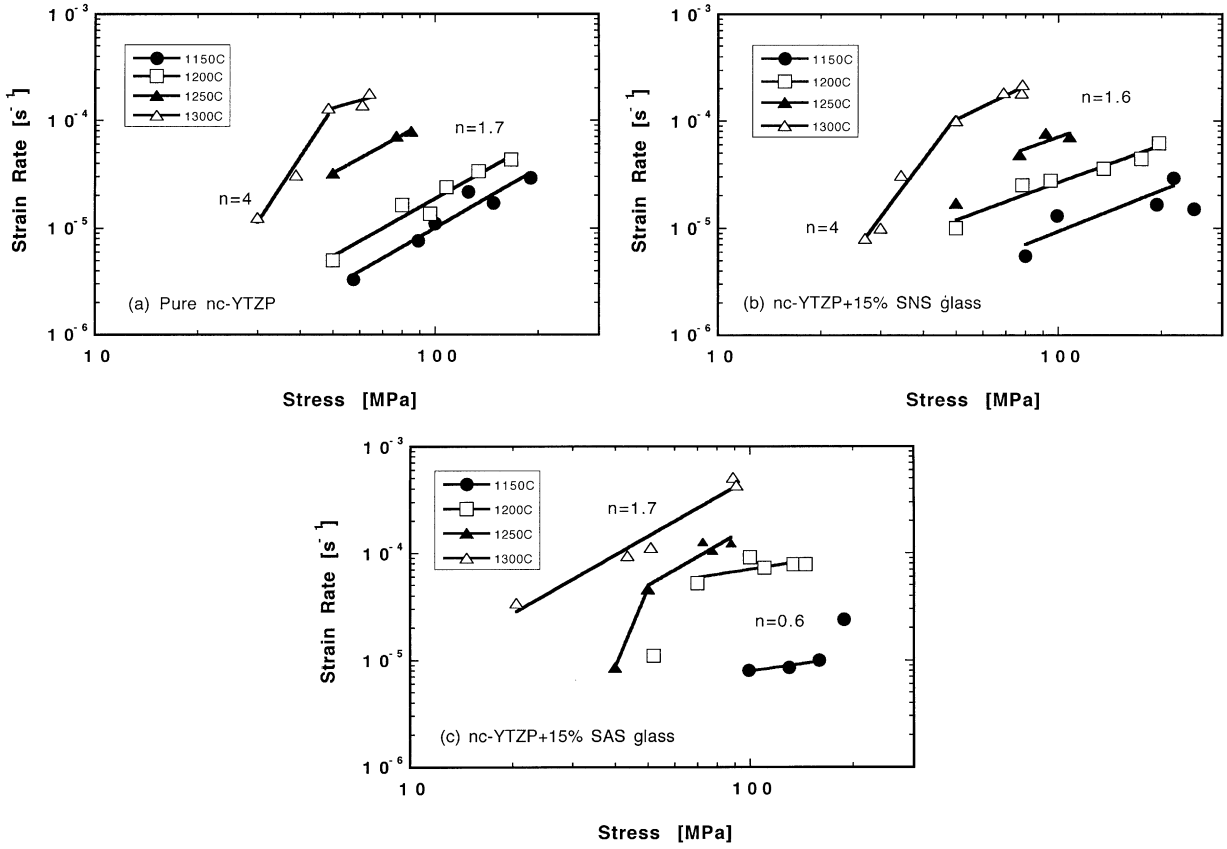

Fig. 1. Strain rate versus stress and temperature dependence of the (a) glass-free nc Y-TZP and alloys containing (b) 15% SNS glass and (c) 15% SAS glass.

The effect of the glass content (vol.%) on the strain rate at 1300 °C for the SNS glass-containing samples is shown in Fig. 2. Samples with higher glass contents (10 and 15 vol.%) revealed similar behavior while their n values changed from 1.6 at higher stresses to 4 at the stresses below 50 MPa. Nevertheless, the n value of the sample with 5 vol.% SNS glass was constant ($n=2.0$) over the applied stress range.

The effect of temperature on the strain rate in the 10 vol.% SAS glass-containing samples is shown in Fig. 3. Compared to the 15 vol.% SAS glass samples (Fig. 1c), decrease in the glass content was found to lower the corresponding strain rate values, but at the same time caused also a change in the deformation mechanism. In this respect, the n values at 1300 and 1200 °C increased to 3.5 and 2.0, respectively (compared to 1.7 and 0.6 in the 15 vol.% glass sample). The overall changes in the n values are summarized in Table 3.

Arrhenius-type plots of the corresponding strain rates (at constant stress) versus reciprocal temperature

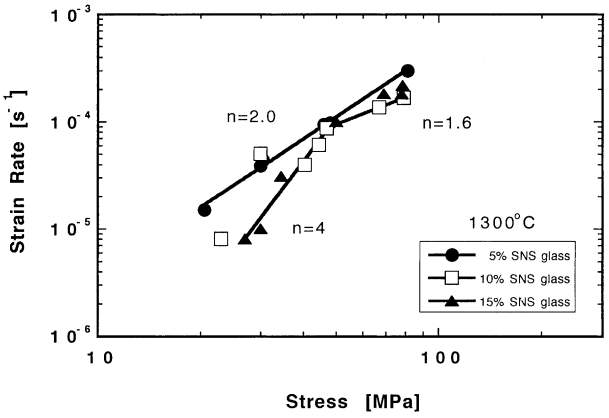

Fig. 2. Effect of the SNS glass content on the strain rate versus stress at 1300 °C.

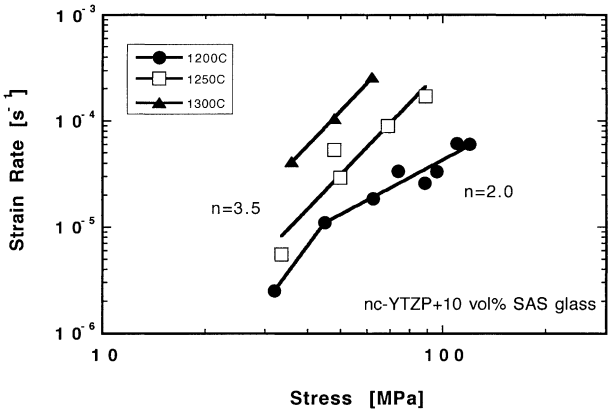

Fig. 3. Effect of the deformation temperature on the strain rate versus stress in the nc-YTZP alloys with 10 vol.% SAS glass.

exhibited linear behavior in the regime where $n \sim 1.6$–2.0 as shown in Fig. 4. Activation energies of 297 ± 15 kJ/mol and 275 ± 15 kJ/mol were determined for the glass-free nc Y-TZP and the glass-containing samples, respectively.

3.2. The microstructure

3.2.1. SEM observations

The microstructure of selected samples prior to and after the deformation were characterized, as indicated in Table 2. SEM observations were performed on two type of surfaces: (a) the surfaces subjected to the compressive stress that were in contact with the compressing pad. (b) Free surfaces that were perpendicular to the surfaces in (a) and subjected to the tensile and shear stresses (Fig. 5). The following series of SEM images represent the microstructure at these two types of surface. Low magnification image of the 15 vol.% SAS glass-containing sample surface in compression deformed at 1300 °C is shown in Fig. 6a and consists of homogeneous microcracks. The microcracks also originated from existing porosities at the surface. SEM observation at higher magnifications (Fig. 6b) revealed that these microcracks were formed along the grain boundaries of the grain clusters. Similar microstructure, albeit with far less crack density, was observed in samples deformed at 1200 °C (Fig. 7a).

However, the surfaces subjected to tensile/shear stresses revealed different microstructure. These surfaces at 1300 °C appeared to be homogeneously corrugated, i.e. the surface roughness was due to many single grains as

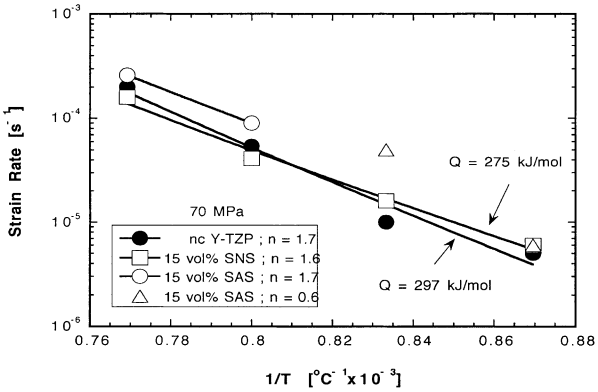

Fig. 4. Activation energies for the plastic deformation at the regime where $n \sim 1.6$–1.7 were determined as 297 ± 15 and 275 ± 15 kJ/mol in the pure and the glass-containing samples, respectively.

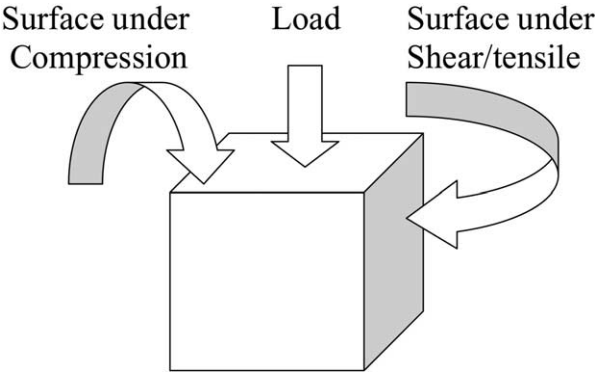

Fig. 5. Schematic description of the loading orientation and the two types of surface examined in SEM after the deformation.

Table 2
Uniaxial deformation test conditions and results

No.	Composition	Designation	Deformation temperature (°C)	Deformation duration (h)	Total strain (%)	Remarks
1	Pure nc-Y-TZP	34/5	1150	3.7	84	
2	Pure nc-Y-TZP	34/6	1200	3.2	75	
3	Pure nc-Y-TZP	34/3	1250	1.3	71	
4	Pure nc-Y-TZP	34/4	1250	1.5	55	**
5	Pure nc-Y-TZP	34/1	1250	2.0	67	
6	Pure nc-Y-TZP	34/5–2	1300	2.8	45	*
7	nc-Y-TZP-5%SNS	42/2	1300	2.4	49	
8	nc-Y-TZP-10%SNS	41/1	1300	3.4	45	
9	nc-Y-TZP-15%SNS	36/5	1150	3.4	89	
10	nc-Y-TZP-15%SNS	36/6	1200	2.6	73	
11	nc-Y-TZP-15%SNS	36/3	1250	3.1	58	**
12	nc-Y-TZP-15%SNS	36/4	1300	4.4	42	*
13	nc-Y-TZP-10%SAS	2/1	1200	>4	63	
14	nc-Y-TZP-10%SAS	2/2	1250	2.7	60	**
15	nc-Y-TZP-10%SAS	2/3	1300	1.5	74	
16	nc-Y-TZP-15%SAS	3/3	1150	2.1	63	
17	nc-Y-TZP-15%SAS	3/2	1200	2.6	55	**
18	nc-Y-TZP-15%SAS	36/1a	1200	2.2	92	
19	nc-Y-TZP-15%SAS	3/4	1250	–	–	
20	nc-Y-TZP-15%SAS	36/1b	1250	2.0	57	
21	nc-Y-TZP-15%SAS	3/1	1300	1.5	38	**

* TEM observation; ** SEM observation.

Table 3
Summary of the n values versus composition-temperature

Composition	1150 °C	1200 °C	1250 °C	1300 °C
Pure nc-Y-TZP	1.7	1.7	1.7	4.0 / 1.7
5 vol.% SNS	–	–	–	2.0
10 vol.% SNS	–	–	–	4.0 / 1.6
15 vol.% SNS	1.6	1.6	1.6	4.0 / 1.6
10 vol.% SAS	–	2.0 / 3.5	3.5	3.5
15 vol.% SAS	0.6	0.6	1.7	1.7

well as grain clusters (Fig. 6c and d). No significant cavitation, crack growth or tearing effects were observed. Few cavities were present and comparable in their size to the grain diameter (Fig. 6d). In contrast, the similar surfaces at 1200 °C exhibited nonhomogeneous microstructure with significant tearing (Fig. 7b). At higher magnifications the absence of homogeneous deformation as well as localized crack growth were clearly visible (Fig. 7c).

SEM images from the compressive and tensile surfaces of the 10 vol.% SAS glass-containing sample deformed at 1250 °C are shown in Fig. 8a and b, respectively. The microstructure at the as-compressed surfaces was fairly flat and contained traces of the glassy phase that apparently detached from the contact surface by way of the compressing pad (Fig. 8a). No pore growth or continuous microcracks were observed. On the other hand, the tensile/shear surfaces (Fig. 8b) exhibited two types of region with different microstructures. First, pore growth and crack opening were observed at the regions buckled upwards from the surface (marked "up" in Fig. 8b). These regions (Fig. 8c) most possibly subjected to high tensile component, perpendicular to the compression axis. Second, the regions which were buckled inwards from the surface (marked "in" in Fig. 8b) were most possibly subjected to a high shear component, in angle to the compression axis. The last regions exhibited a unique microstructure of grain clusters that slipped over each other (Fig. 8d). To our best knowledge, this microstructural observation is the first evidence in the published literature that confirms the validity of the cooperative grain boundary sliding mechanism[14] in ceramics. High magnification image of such a region (Fig. 8e) clearly revealed that the clusters contain nanometer-size grains. This finding is in agreement with previous microstructural observation of the sintered samples,[12,13] where the glass did not promote grain growth.

Comparison of the microstructures developed in the last three samples indicates that excess glass may be detrimental in providing 'weak' sites for cavity nucleation under the tensile stresses. Consequently, the volume fraction of the glass needs to be optimized.

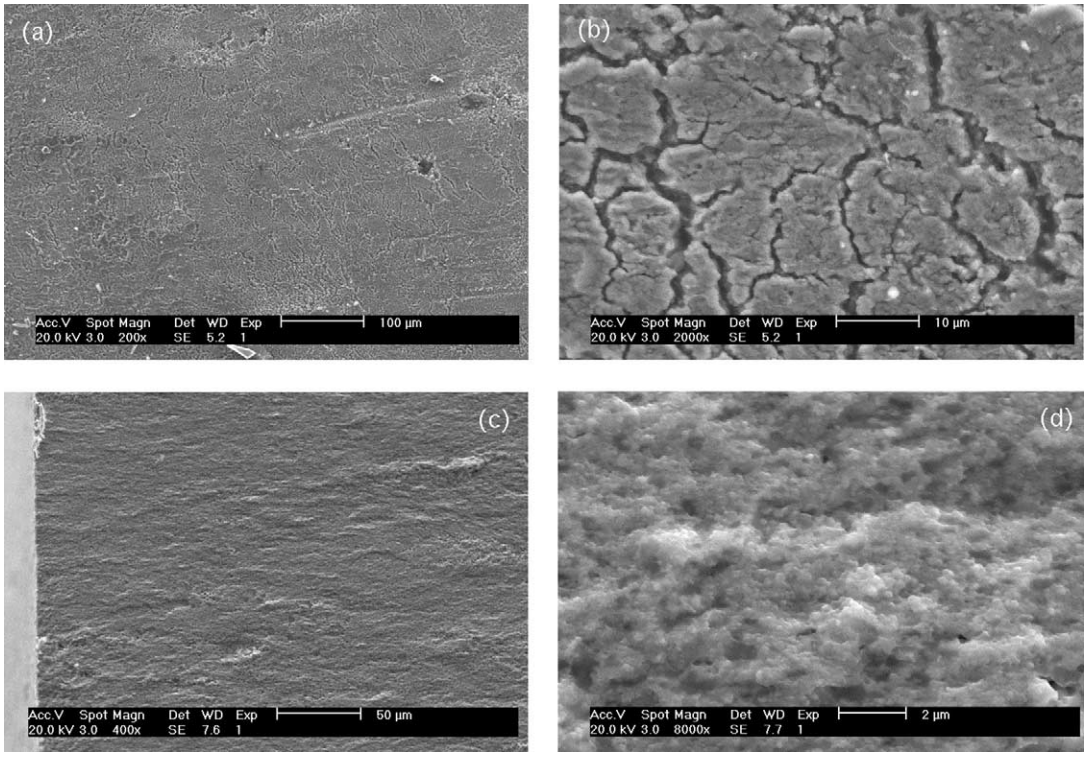

Fig. 6. SEM images from the surfaces (a) and (b) under compression, and (c) and (d) under tensile/shear stresses. 15% SAS glass-containing nc-Y-TZP deformed at 1300 °C. The compression direction is along the vertical axis in (c) and (d).

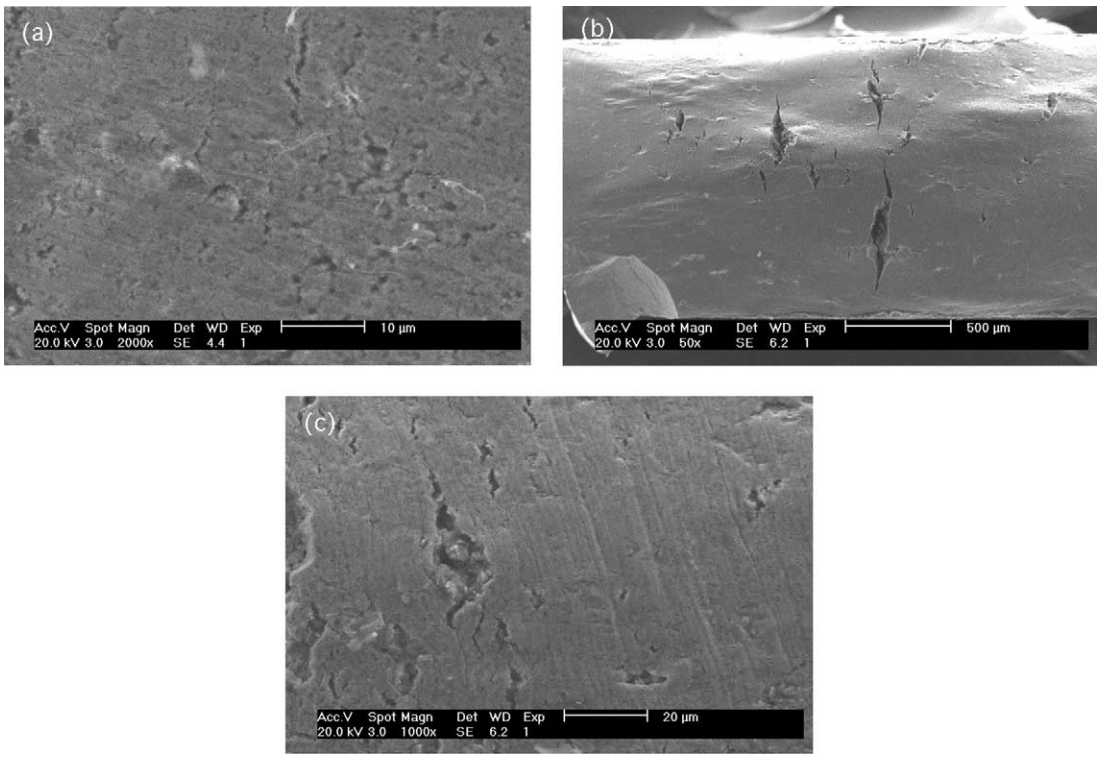

Fig. 7. SEM images from the surfaces (a) under compression, and (b) and (c) under tensile/shear stresses. 15% SAS glass-containing nc-Y-TZP deformed at 1200 °C. The compression direction is along the vertical axis in (b) and (c).

SEM images from the surfaces under compression in the 15 vol.% SNS glass-containing sample deformed at 1250 °C are shown in Fig. 9. The low magnification image (Fig. 9a) revealed a microcrack pattern similar to that found in the 15 vol.% SAS counterpart sample (Fig. 6a). Images at higher magnifications showed that these microcracks were developed and propagated along the grain boundaries (Fig. 9b). Observation at the tensile/shear surfaces (Fig. 9c) revealed a complex microstructure that was composed of homogeneous microcracks (perpendicular to the tensile stress direction) and shear bands (parallel to the tensile stress and perpendicular to the surface). At higher magnifications (Fig. 9d) the shear bands could be seen to consist of nanocrystalline grains. Nevertheless, this microstructure was not typical for the cooperative grain boundary sliding.

Appropriate SEM images from the pure (glass-free) nc-Y-TZP samples deformed at 1250 °C (as a reference sample) are shown in Fig. 10. Homogeneous microcracking was also observed at the compressive surfaces of this sample (Fig. 10a). However, the tensile/shear surfaces contained traces of parallel straight lines, typical for slip bands (Fig. 10b). At higher magnifications, these bands were found to be composed of nanocrystalline grains (Fig. 10c) apparently slipped over each other (no cooperative grain boundary sliding was observed). This microstructure represents plastic deformation by a grain boundary sliding mechanism.

3.2.2. TEM observations

Typical TEM images from the as-sintered samples prior to the deformation showed equiaxed grains, either with faceted grain boundaries (Fig. 11a) (in glass-free nc-Y-TZP) or spherical grains surrounded by the glassy layer (Fig. 11b) (in glass-containing Y-TZP's). Increase in the glass content caused an increase in the roundness of the zirconia grains as has been reported previously.[12]

The microstructure of the pure, glass-free nc-Y-TZP as well as that with 15 vol.% SNS glass after more than 40% plastic deformation are shown in Fig. 12a and b, respectively. Generally, the microstructures of the deformed specimens were identical to those prior to the deformation with respect to grain size and morphology. The main difference was formation of twins which may occur for stress relaxation or due to the martensitic phase transformation of the tetragonal grains to the monoclinic symmetry (during the cooling). No dislocations were resolvable due to the heavily twinned nature of the monoclinic grains. On the other hand, in the twin-free tetragonal grains, also no dislocation activity was found, irrespective of the sample composition. In addition, the glass-containing samples exhibited pore growth and the grains were rounded (Fig. 12b). These findings do not add more information to the understanding of the deformation mechanism but confirm the grain boundary sliding to be the dominant deformation mechanism in these alloys.

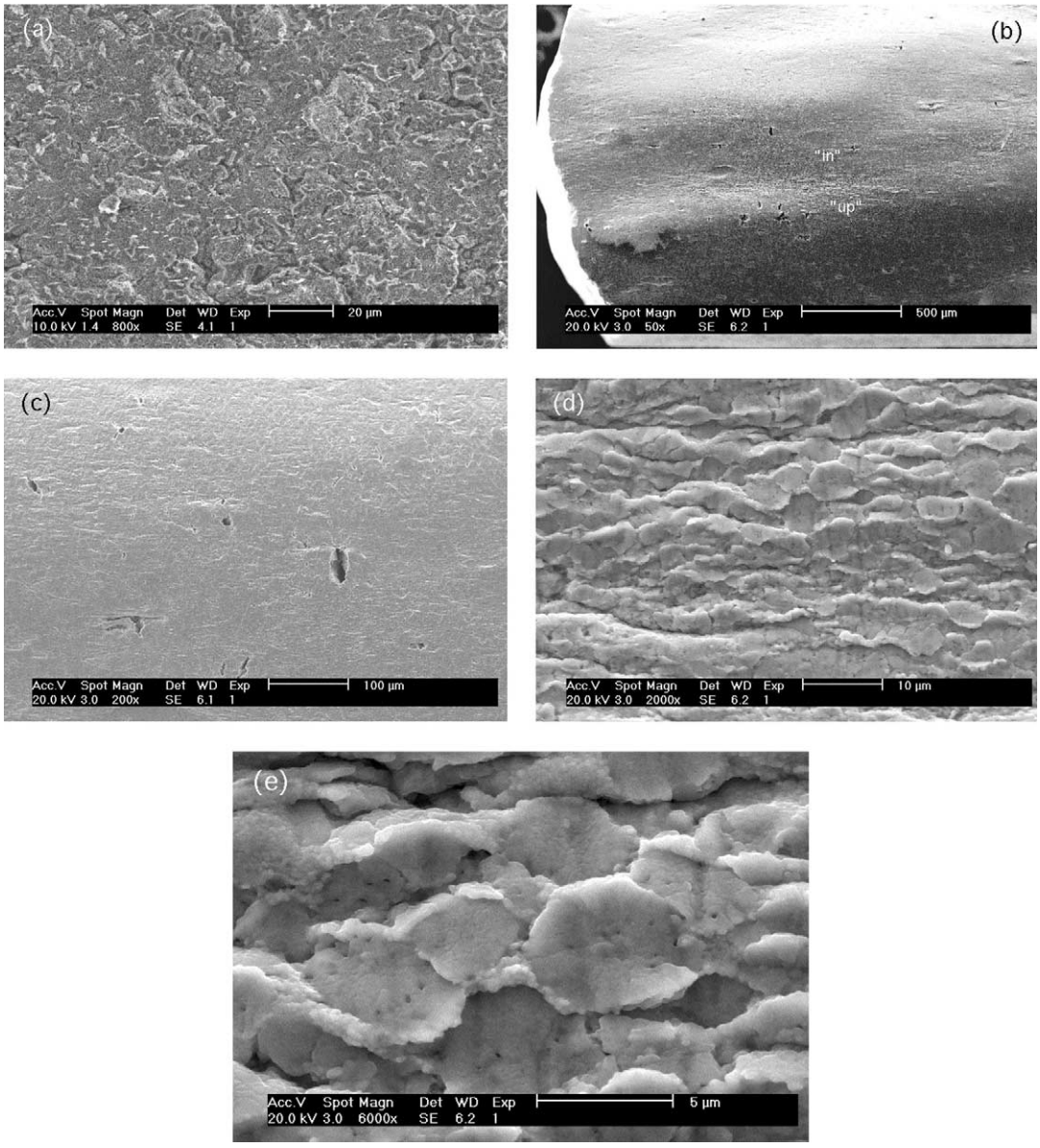

Fig. 8. SEM images from the surfaces (a) under compression, and (b) to (e) under tensile/shear stresses. 10 vol.% SAS glass-containing nc-Y-TZP deformed at 1250 °C. The compression direction is along the vertical axis in (b) through (e). See the text for further explanation.

4. Discussion

Superplastic deformation was reported by many investigators for submicron grain size Y-TZP's having different impurity contents.[15–24] Comparison of the present data to those in the literature shows that the n values found here are comparable to the range of the n values (1.3–3.8) reported for the submicron grain size Y-TZP systems.[6] A variety of strain-rate controlling mechanisms such as solution-reprecipitation, interface reaction controlled creep, grain boundary sliding accommodated by intragranular slip and others have been postulated to be operative. Nevertheless, it was shown by Dominguez et al.[25] that a single deformation mechanism could be used to explain the plastic deformation in submicron Y-TZP ceramics, assuming a threshold stress. In this respect, low purity samples exhibit $n=2$ whereas higher purity samples exhibit transition from $n \cong 2$ to values higher than 3 for decreasing stress. It should be noted that $n=2$ is the 'natural' exponent for superplastic deformation in metals. Therefore, the n values above 1.5 in the present research could be related to the diffusive grain boundary sliding mechanism.[26] In this respect, the Gifkins' mantle model[27] is the most feasible for description of the deformation mechanism in the present samples, as originally suggested by Okamoto et al.[28] This model is in agreement with the morphological changes that were observed at the tensile/shear surfaces of the deformed samples.

The value of the exponent n was found to increase to high values (between 3 and 4) at the transition stress on

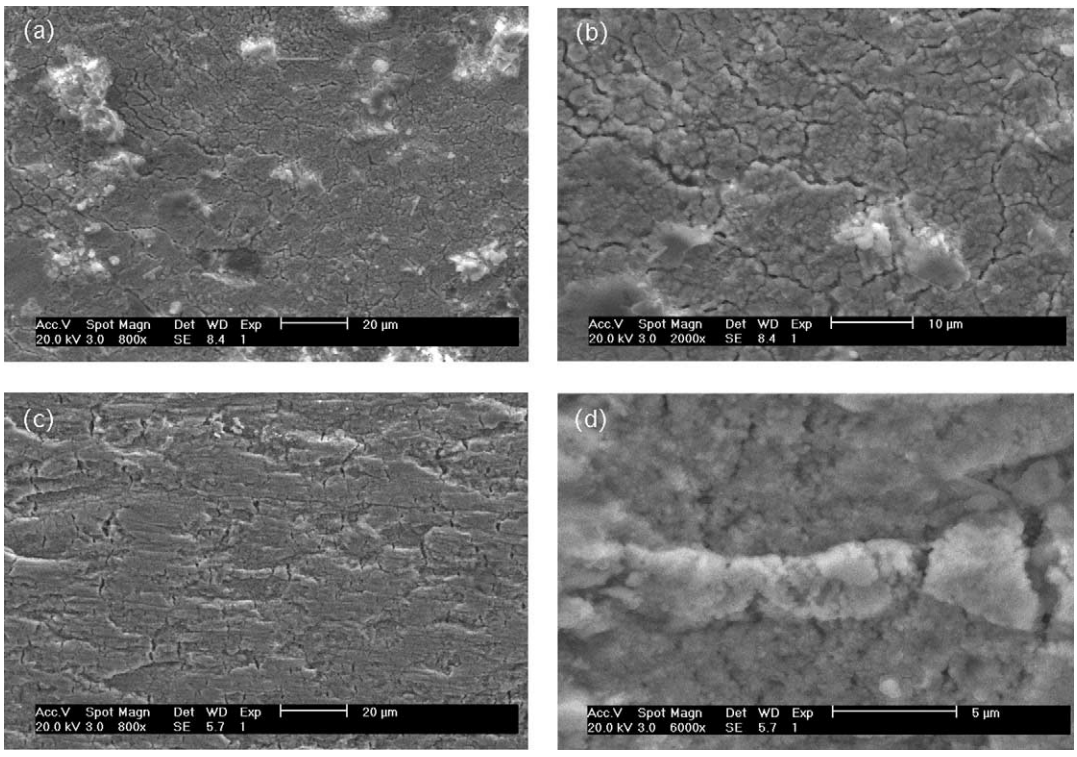

Fig. 9. SEM images from the surfaces (a) and (b) under compression, and (c) and (d) under tensile/shear stresses. 15% SNS glass-containing nc-Y-TZP deformed at 1250 °C. The compression direction is along the vertical axis in (c) and (d).

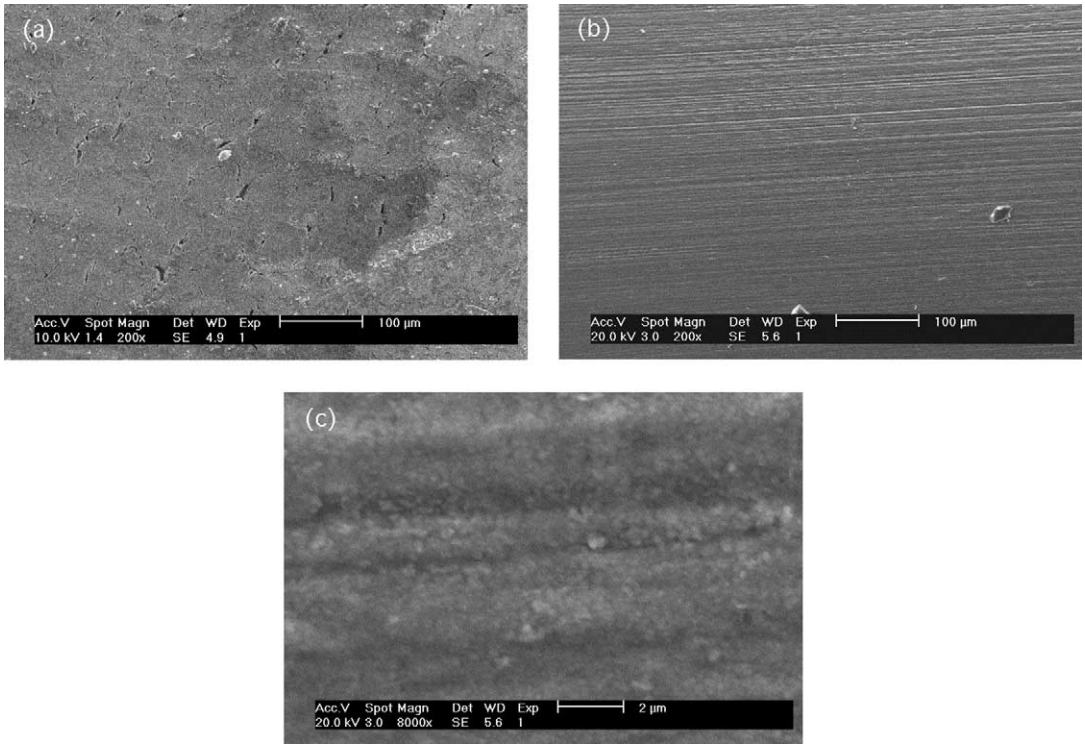

Fig. 10. SEM images from the surfaces (a) under compression, and (b) and (c) under tensile/shear stresses. Glass-free nc-Y-TZP deformed at 1250 °C. The compression direction is along the vertical axis in (b) and (c).

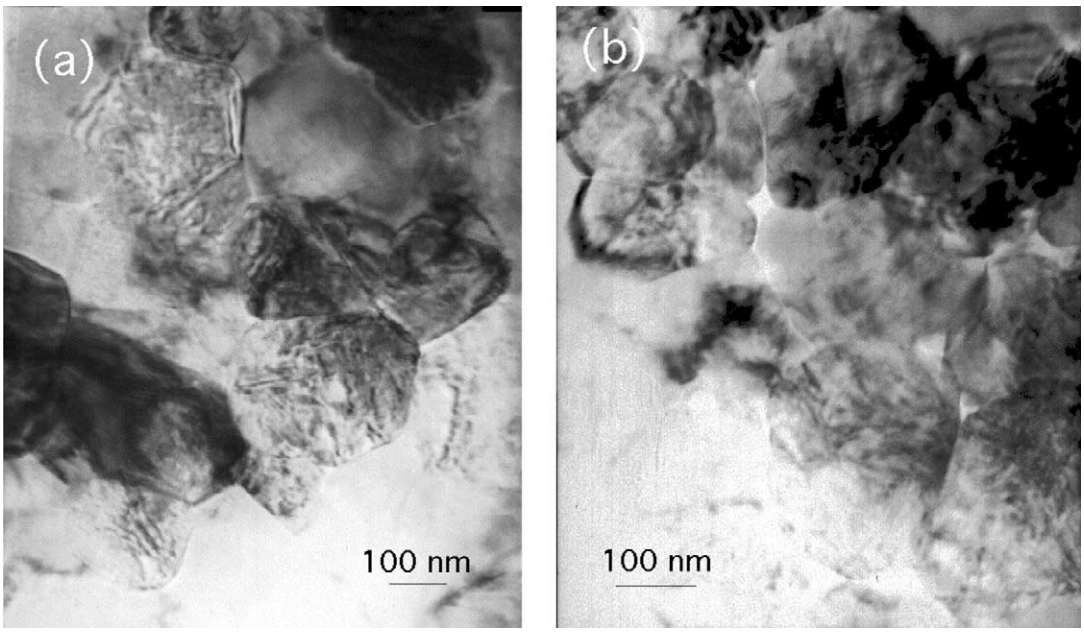

Fig. 11. TEM images from the as-sintered samples prior to the high temperature plastic deformation. (a) Faceted equiaxed grains in the glass-free nc-Y-TZP. (b) Rounded grains in the 15 vol.% SNS glass-containing sample.

lowering the stress. Nevertheless, this transition occured in the pure as well as in the SNS glass-containing nc-Y-TZP samples only at 1300 °C at stresses of about 50 MPa. In the SAS glass-containing samples, this transition occured already at 1200 °C.

On the other hand, as the n values tend to decrease towards 1.0, one can expect a linear dependence of the strain rate with stress. This type of behavior is consistent with grain boundary sliding aided by either Newtonian viscous flow in the glass-containing samples or by diffusional creep[28] in the pure submicron size Y-TZP.

The lowest n value of 0.6 which was observed in the 15 vol.% SAS glass-containing samples deformed at lower temperatures may be explained by the non-Newtonian viscous flow of the sample, by which the viscosity dependence on the shear stress is parabolic. However,

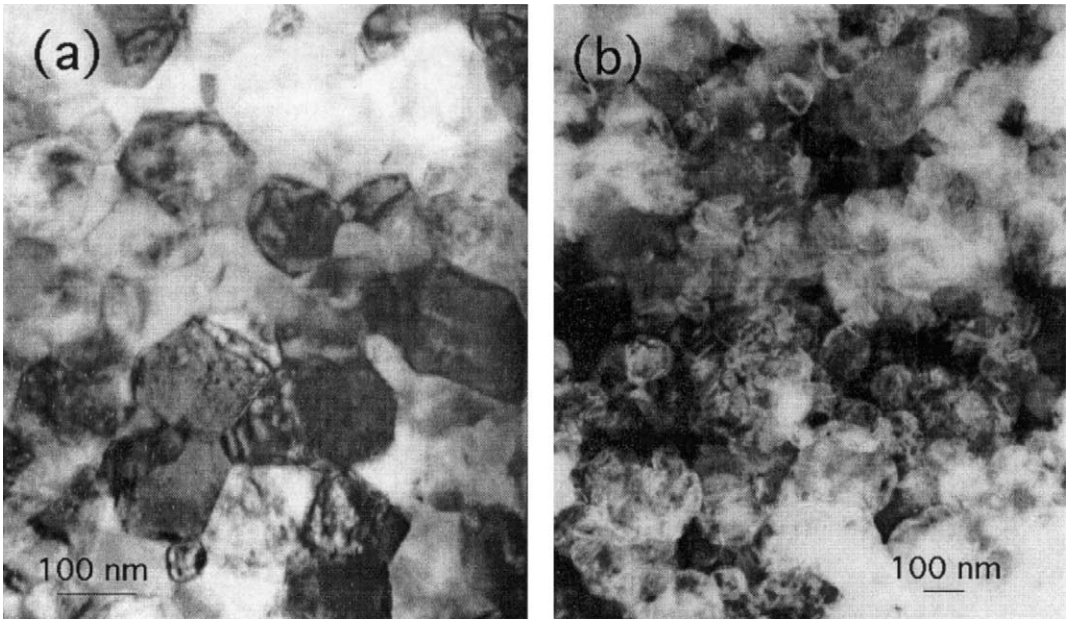

Fig. 12. TEM images from the samples after more than 40% plastic deformation. (a) glass-free nc-Y-TZP. (b) 15% SNS glass-containing sample. The microstructures are similar to those prior to the deformation as in Fig. 11.

verification of this postulate necessitates characterization of the viscosity of the grain boundary glassy phase.

The published activation energies for superplastic deformation in Y-TZP ceramics span a wide range of values, i.e. from 360 to 720 kJ/mol.[6,29] Activation energy of ~500 kJ/mol is often reported for creep experiments of coarse-grained Y-TZP.[15] The activation energy in the glass-free and the SNS glass-containing samples is very close to that for the grain boundary diffusion of cations (290 kJ/mol for Y^{3+} and 310 kJ/mol for Zr^{4+}).[30,31] The corresponding activation energies for the bulk diffusion of the same cations were measured, by way of diffusion experiments as 460 kJ/mol and 510 kJ/mol for Y^{3+} and Zr^{4+}, respectively.[32,33] In addition, the activation energy for viscous flow in the silica-based glasses (i.e. diffusion in viscous silica) is about ~190 kJ/mol. Comparison of the measured activation energy (297±15 and 275±15 kJ/mol) to the data from the literature indicates that the plastic deformation mechanisms are controlled primarily by the grain boundary diffusion processes. Nevertheless, in pure glass-free nc-Y-TZP samples the deformation rate is controlled by diffusion of either Y^{+3} or Zr^{+4} cations along the grain boundaries. On the other hand, appropriate calculations for the impure nc-Y-TZP ceramics have shown the interface reaction controlled processes (at the glass/crystal interfaces) to be rate controlling rather than the diffusion processes within the glass.[11] Addition of appropriate glass, i.e. SAS glass in the present investigation, has led to the change in the deformation mechanism as was evidenced at lower deformation temperatures.

In this respect, the mutual solubility between the glassy phase and the Y-TZP grains may change significantly at high temperatures.[34] Apparently, the SAS glass has lower solubility (due to the Al_2O_3 content) than the SNS glass in the zirconia grains. Therefore, one may expect the superplastic strain rate to depend on the solubility of the glass at the deformation temperature. This effect may change, in turn, the superplastic deformation mechanism as was observed here.

5. Summary and conclusions

Nanocrystalline Y-TZP ceramics containing 5–15 vol.% of two different glass compositions were uniaxially deformed at different temperature-stress conditions. The dependence of the strain rate on temperature, stress, glass content and its composition were determined. The highest strain rates were observed for the SAS glass-containing samples. The deformed microstructures clearly confirmed cooperative grain boundary sliding as well as grain boundary sliding mechanisms to be operative in the glass-containing and the glass-free nc-Y-TZP samples, respectively.

Acknowledgements

The authors thank the Israel Ministry of Science, Culture and Sports for supporting this research through the infrastructure grant #1090–1-98.

References

1. Wakai, F., Sakaguchi, S. and Matsuno, Y., Superplasticity of yttria-stabilized tetragonal ZrO_2 polycrystals. *Adv. Ceram. Mater*., 1986, **1**, 259–263.
2. Nieh, T. G., McNally, C. M. and Wadsworth, J., Superplastic behavior of a yttria-stabilized tetragonal zirconia polycrystal. *Scripta Metall*., 1988, **22**, 1297–1300.
3. Nieh, T. G., Wadsworth, J. and Sherby, O. D., *Superplasticity in Metals and Ceramics*. Cambridge Solid State Science Series, Cambridge, 1997 pp. 91–99.
4. Gutierrez-Mora, F., Dominguez-Rodriguez, A., Jimenez-Melendo, M., Chaim, R., Ravi, B. G. and Routbort, J. L., Current understanding of superplastic deformation of Y-TZP and its application to joining. *Mater. Sci. Eng. A*, 2001, **302**, 154–161.
5. Gutierrez-Mora, F., Dominguez-Rodriguez, A., Jimenez-Melendo, M., Chaim, R. and Hefetz, M., Creep of nanocrystalline Y-SZP ceramics. *NanoStruct. Mater*., 1999, **11**, 531–537.
6. Jimenez-Melendo, M., Dominguez-Rodriguez, A. and Bravo-Leon, A., Superplastic flow of fine-grained yttria-stabilized zirconia polycrystals: constitutive equation and deformation mechanisms. *J. Am. Ceram. Soc*., 1998, **81**, 2761–2776.
7. Chokshi, A. H., Superplasticity in fine-grained ceramic and ceramic composites: current understanding and future prospects. *Mater. Sci. Eng. A*, 1993, **166**, 119–133.
8. Langdon, T. G., The characteristics of superplastic-like flow in ceramics. In *Plastic deformation of ceramics*, ed. R. C. Bradt, C. A. Brooks and J. L. Routbort. Plenum press, New York, 1995, pp. 251–268.
9. Pharr, G. M. and Ashby, M. F., On creep enhanced by a liquid phase. *Acta Metall*., 1983, **31**, 129–138.
10. Dryden, J. R., Kucerovsky, D., Wilkinson, D. S. and Watt, D. F., Creep deformation due to a viscous grain boundary phase. *Acta Metall*., 1989, **37**, 2007–2015.
11. Chaim, R., Plastic deformation in impure nanocrystalline ceramics. *J. Mater. Res*., 1999, **14**, 2508–2517.
12. Ramamoorthy, R. and Chaim, R., Sintering and microstructure of glass-coated nanocrystalline Y-TZP powder: Effect of the glass. *J. Mater. Res*., 2001, **16**(1), 296–302.
13. Ramamoorthy, R. and Chaim, R., Microstructural evolution in the nanocrystalline Y-TZP containing a silicate glass, *J. Eur. Ceram. Soc*. (in press).
14. Zelin, M. G., Cooperative grain boundary sliding in materials with non-uniform microstructure. *J. Mater. Sci. Lett*., 1996, **15**, 2068–2070.
15. Hwang, C.-M. J. and Chen, I-W., Effect of a liquid phase on superplasticity of 2-mol%-Y_2O_3-stabilized tetragonal zirconia polycrystals. *J. Am. Ceram. Soc*., 1990, **73**, 1626–1632.
16. Yoshizawa, Y.-I. and Sakuma, T., Role of grain-boundary glass phase on the superplastic deformation of tetragonal zirconia polycrystal. *J. Am. Ceram. Soc*., 1990, **73**, 3069–3073.
17. Gust, M., Goo, G., Wolfenstine, J. and Mecartney, M. L., Influence of amorphous grain boundary phases on the superplastic behavior of 3-mol%-yttria-stabilized tetragonal zirconia polycrystals (3Y-TZP). *J. Am. Ceram. Soc*., 1993, **76**, 1681–1690.
18. Rouxel, T. and Wakai, F., The brittle to ductile transition in a Si_3N_4/SiC composite with a glassy grain boundary phase. *Acta Metall. Mater*., 1993, **41**, 3203–3213.

19. Seidensticker, J. R. and Mayo, M. J., *Scripta Metall. Mater.*, 1994, **31**, 1749–1754.
20. Kajihara, K., Yoshizawa, Y. and Sakuma, T., The enhancement of superplastic flow in tetragonal zirconia polycrystals with SiO_2-doping. *Acta Metall. Mater.*, 1995, **43**, 1235–1242.
21. Shi, J. L., Zhu, G. Q. and Lai, T. R., Compressive deformation behaviour of superplastic Y-TZP based ceramics: Role of grain boundary phases. *J. Eur. Ceram. Soc.*, 1997, **17**, 851–858.
22. Tekeli, S. and Davies, T. J., Influence of a transition metal oxide (CuO) on the superplastic behaviour of 8 mol% yttria-stabilised cubic zirconia polycrystal (8Y-CSZ). *J. Mater. Sci.*, 1998, **33**, 3267–3273.
23. Thavorniti, P., Ikuhara, Y. and Sakuma, T., Microstructural characterization of superplastic SiO_2-doped TZP with a small amount of oxide addition. *J. Am. Ceram. Soc.*, 1998, **81**, 2927–2932.
24. Chen, L., Rouxel, T., Chaim, R., Vesteghem, H. and Sherman, D., Superplasticity and creep in monoclinic and Y-PSZ nanograined zirconia. *Mater. Sci. Forum*, 1997, **243–245**, 245–250.
25. Bravo-Leon, A., Jimenez-Melendo, M., Dominguez-Rodriguez, A. and Chokshi, A. H., The role of a threshold stress in the superplastic deformation of fine-grained yttria-stabilized zirconia polycrystals. *Scripta Mater.*, 1996, **34**(7), 1155–1160.
26. Badwall, S. P. S., Ciacchi, F. T., Swain, M. V. and Zelizko, V., Creep deformation and the grain-boundary resistivity of tetragonal zirconia polycrystalline materials. *J. Am. Ceram. Soc.*, 1990, **73**(8), 2505–2507.
27. Gifkins, R. C., Grain-boundary sliding and its accomodation during creep and super-plasticity. *Met. Trans.*, 1976, **7A**(8), 1225–1232.
28. Okamoto, Y., Ieuji, J., Yamada, Y., Hayashi, H., and Nishikawa, T., Creep deformation of yttria-stabilized tetragonal zirconia (Y-TZP). In: Somiya, S., Yamamoto, N. and Yanagida, H., Advances in Ceramics, Vol. 24, ACerS, Westerville, Ohio (1988) pp.565–71.
29. Evans, P. E., Creep in yttria- and scandia-stabilized zirconia. *J. Am. Ceram. Soc.*, 1970, **53**(7), 365–369.
30. Sakka, Y., Oishi, Y. and Ando, K., Zr-Hf interdiffusion in polycrystalline Y_2O_3-$(Zr+Hf)O_2$. *J. Mater. Sci.*, 1982, **17**, 3101–3105.
31. Oishi, Y., Ando, K. and Sakka, Y., Lattice and grain-boundary diffusion coefficients of cations in stabilized zirconias. In *Advances in Ceramics, Vol. 7*, ed. M. F. Yang and A. H. Heuer. ACerS, Columbus, Ohio, 1983, pp. 208–219.
32. Solmon, H., Chamat, J., Dolin, C. and Monty, C., Zr, Y and O self-diffusion in $Zr_{1-x}\ Y_xO_{2-x/2}$ ($x=0.17$). In *Ceramic Transactions, Vol. 24*, ed. T. O. Mason and J. L. Routbort. ACerS, Westerville, Ohio, 1991.
33. Chien, F. R. and Heuer, A. H., Lattice diffusion kinetics in Y_2O_3-stabilized cubic-ZrO_2 single crystals: a dislocation loop annealing study. *Philos. Mag. A*, 1996, **73**(3), 681–699.
34. Ikuhara, Y., Nagai, Y., Yamamoto, T. and Sakuma, T., High-temperature behavior of SiO_2 at grain boundaries in TZP. *Interface Sci.*, 1999, **7**, 77–84.